BIOCHEMISTRY
including biophysical chemistry & molecular biology

Article

pubs.acs.org/biochemistry

Rational Modulation of the Induced-Fit Conformational Change for Slow-Onset Inhibition in *Mycobacterium tuberculosis* InhA

Cheng-Tsung Lai,[†,‡] Huei-Jiun Li,[†] Weixuan Yu,[§] Sonam Shah,[§] Gopal R. Bommineni,[§] Victoria Perrone,[§] Miguel Garcia-Diaz,[∥] Peter J. Tonge,[*,†,§,⊥] and Carlos Simmerling[*,†,‡,§,⊥]

[†]Graduate Program in Biochemistry and Structural Biology, [‡]Laufer Center for Physical and Quantitative Biology, [§]Department of Chemistry, [∥]Department of Pharmacological Sciences, and [⊥]Institute for Chemical Biology & Drug Discovery, Stony Brook University, Stony Brook, New York 11794, United States

Supporting Information

ABSTRACT: Slow-onset enzyme inhibitors are the subject of considerable interest as an approach to increasing the potency of pharmaceutical compounds by extending the residence time of the inhibitor on the target (the lifetime of the drug−receptor complex). However, rational modulation of residence time presents significant challenges because it requires additional mechanistic insight, such as the nature of the transition state for postbinding isomerization. Our previous work, based on X-ray crystallography, enzyme kinetics, and molecular dynamics simulation, suggested that the slow step in inhibition of the *Mycobacterium tuberculosis* enoyl-ACP reductase InhA involves a change in the conformation of the substrate binding loop from an open state in the initial enzyme−inhibitor complex to a closed state in the final enzyme−inhibitor complex. Here, we use multidimensional free energy landscapes for loop isomerization to obtain a computational model for the transition state. The results suggest that slow-onset inhibitors crowd key side chains on helices that slide past each other during isomerization, resulting in a steric clash. The landscapes become significantly flatter when residues involved in the steric clash are replaced with alanine. Importantly, this lower barrier can be increased by rational inhibitor redesign to restore the steric clash. Crystallographic studies and enzyme kinetics confirm the predicted effects on loop structure and flexibility, as well as inhibitor residence time. These loss and regain of function studies validate our mechanistic hypothesis for interactions controlling substrate binding loop isomerization, providing a platform for the future design of inhibitors with longer residence times and better *in vivo* potency. Similar opportunities for slow-onset inhibition via the same mechanism are identified in other pathogens.

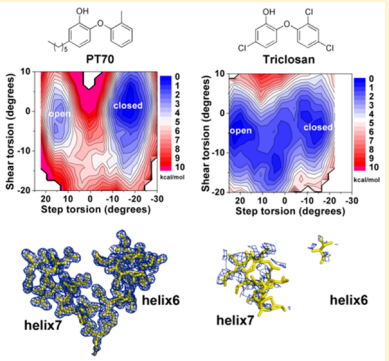

Recently, kinetic parameters have emerged as important metrics of drug efficacy in the drug discovery field, and an increasing number of studies have emphasized structure−kinetics relationships.[1−5] Traditionally, equilibrium dissociation constants determined *in vitro* (such as K_d and IC_{50}) are used to predict *in vivo* efficacy. However, *in vivo* concentrations of the inhibitor and target typically vary with time. Thus, equilibrium properties alone may be inadequate predictors of *in vivo* efficacy. Residence time, the reciprocal of the dissociation rate constant, represents the lifetime of an enzyme−inhibitor complex and has become an important additional parameter in lead optimization.[6,7] In particular, a study of *Francisella tularensis* FabI inhibitors revealed that *in vivo* efficacy has better correlation with residence time than with thermodynamic binding affinity.[8] The observation that many currently marketed drugs have long residence times on their targets further suggests that drug−target residence time is an important component of *in vivo* drug activity.[9] To validate the role of residence time in modulating drug activity, systems in which the mechanistic basis of residence time is understood and can be rationally altered are needed. We recently showed that the *Mycobacterium tuberculosis* (MTB) enoyl-ACP reductase InhA is an excellent system for investigating the structural and energetic basis of long residence times. Kinetic, crystallographic, and computational data were used to develop a model in which slow-onset inhibition of InhA arises from a two-step induced-fit binding mechanism (Scheme 1), wherein induced-fit isomerization of the substrate binding loop (SBL) is the slow step for inhibitors with long residence times.[18]

Here, we investigate the underlying structural and energetic basis for SBL isomerization kinetics and show that the free energy landscape of the SBL isomerization not only can be understood but also can be rationally controlled through targeted variation of amino acids on the SBL, or by modifying the structure of the inhibitor.

Scheme 1

$$E+I \underset{k_4}{\overset{k_3}{\rightleftharpoons}} EI \underset{k_6}{\overset{k_5}{\rightleftharpoons}} EI^*$$

Received: March 16, 2015
Revised: July 6, 2015
Published: July 6, 2015

DOI: 10.1021/acs.biochem.5b00284
Biochemistry 2015, 54, 4683−4691

Isoniazid (INH), a front-line drug used clinically to treat tuberculosis, forms an INH−NAD adduct after activation by KatG. The INH−NAD adduct is a slow-onset inhibitor of InhA, which catalyzes the reduction of *trans*-2-enoyl-ACP in the type II fatty acid biosynthesis (FAS II) pathway.[11] Triclosan, a widely used antimicrobial agent, inhibits InhA directly, but triclosan is a weak binding (K_i = 0.2 μM), rapid-reversible inhibitor of InhA.[12,13] A triclosan variant [2-(*o*-tolyoxy)-5-hexylphenol (PT70)] was developed and shown to be a slow-onset, tight binding inhibitor of InhA[14] with a K_i* value of 0.6 nM and a residence time of 40 min. Structurally, complexes formed of InhA, NAD^+, and either rapid-reversible or slow-onset inhibitors are distinguished on the basis of the structure of helices 6 (residues 197−207) and 7 (residues 211−225) on the SBL.[18] Helix 6 is frequently disordered in enzyme−inhibitor complexes formed by binding of substrate analogues or rapid-reversible inhibitors[12,14,15] but can also be ordered, occupying an open structure that we propose is also characteristic of the initial enzyme−inhibitor complex (EI) formed by slow-onset inhibitors. For the latter, helix 6 subsequently moves to a closed state to generate the final enzyme−inhibitor complex (EI*). This conformational change from the open state to the closed state was hypothesized to be the slow isomerization step as described in the two-step enzyme inhibition mechanism.[18]

In principle, increasing the inhibitor residence time (or dissociation energy barrier) can be approached either by stabilizing the final EI* complex or by destabilizing the transition state between EI and EI* states. Tight binding inhibitors like PT70 present a challenge to further stabilizing the EI* state; thus, destabilization of the transition state could be a more feasible approach to slowing the dissociation kinetics. A model for the transition state to SBL isomerization would then provide valuable insight into rational control of the energy barrier, but these states are inherently difficult to characterize experimentally. Computational studies are often better suited to modeling rare events and can provide direct connections between structure and energy. Our previous work used a variant of the nudged elastic band simulation method (NEB)[16,17] to generate a structural model representing the conformational transition pathway between the crystallographic open and closed states, followed by multidimensional free energy calculations along the path that showed differences in loop flexibility in the presence of rapid-reversible versus slow-onset inhibitors. Here we use the energy landscapes to construct a simulation-based structural model for the transition state to SBL isomerization. This model suggests a mechanism for the differences between rapid-reversible and slow-onset inhibitors and allows rational control of the SBL isomerization.

METHODS

The methods were adopted from our previous study,[18] with further details provided in the Supporting Information. Simulations were conducted with full atomic detail, including explicit water using the Amber software.[19] Amber ff99SB[20] and GAFF[21] force fields were assigned to the protein and inhibitors, respectively, with inhibitor force field parameters provided in Tables S1 and S2 of the Supporting Information. Initial structures for the SBL isomerization end points with PT70 were taken from our previous study.[18] Initial poses of PT163 were generated using DOCK 6.3.[22] Flexible ligand docking was performed with default parameters. We assumed that the diphenyl ether common to PT163 and PT70 would occupy similar positions in the binding pocket; thus, the results with lowest root-mean-square deviation value in the diphenyl ether moiety as compared to the PT70 end point structure was chosen as the initial pose for PT163. For each system, PNEB[17] with simulated annealing was used to map the isomerization pathway. This was followed by two-dimensional (2D) umbrella sampling (500 ps for each of 192 windows) at 300 K along the PNEB path to obtain the free energy landscape. Reaction coordinates for the free energy maps were described previously and included step and shear torsions for helices 6 and 7 (Figure S1 of the Supporting Information). Three-step soft core thermodynamic integration with 19 λ windows was used to calculate binding affinity changes. The one-dimensional (1D) PMFs were obtained from the 2D PMF by measuring the average step and shear torsions for each bead at the end of PNEB optimization, followed by retrieving the free energy values at the corresponding points on the 2D PMF.

Inhibition of InhA by the diphenyl ethers occurs through a two-step induced-fit mechanism. Progress curve kinetics were determined on a Cary 100 UV−vis spectrophotometer (Varian) at 20 °C. Reaction velocities were measured by monitoring the oxidation of NADH to NAD^+ at 340 nm. The enzyme reaction was initiated by adding 75 nM InhA variant to the reaction buffer [30 mM PIPES (pH 6.8), 150 mM NaCl, and 1 mM EDTA] containing *trans*-2-Oct-CoA (200 μM), NADH (250 μM), NAD^+ (200 μM), DMSO [2% (v/v)], inhibitor (0−4000 nM), and 8% glycerol. The reaction was monitored until the progress curve became linear, suggesting that the steady state had been reached. High concentrations of substrate and low concentrations of enzyme were used to minimize substrate consumption and ensure that progress curves remained linear in the absence of inhibitor. The progress curves were analyzed using the Morrison and Walsh integrated rate equation (eq 1) for slow binding inhibition

$$A_t = A_0 - v_s t - (v_i - v_s)\frac{1 - e^{-k_{obs}t}}{k_{obs}} \quad (1)$$

where A_t and A_0 are the absorbance at time t and time zero, respectively, v_i and v_s are the initial velocity and steady state velocity, respectively, and k_{obs} is the pseudo-first-order rate constant for the approach to the steady state.[23,24] k_{off}, which corresponds to the dissociation rate constant of the inhibitor, was calculated via eq 2:

$$k_{off} = k_{obs}\frac{v_s}{v_i} \quad (2)$$

k_6 was assumed to be the rate-limiting step formation of free, active enzyme (Scheme 1), so $k_{off} = k_6$.

K_i^{app}, the apparent dissociation constant for the initial encounter complex (EI), was determined by plotting the fractional initial velocities as a function of inhibitor concentration and fitting to eq 3:

$$\frac{v_i}{v_0} = \frac{1}{1 + \frac{[I]}{K_i^{app}}} \quad (3)$$

where v_0 is the control velocity, from the uninhibited progress curve. K_i^{*app}, the apparent dissociation constant for the final (steady state) EI* complex, was determined by plotting the fractional steady state velocities as a function of inhibitor concentration and fitting to eq 4:

DOI: 10.1021/acs.biochem.5b00284
Biochemistry 2015, 54, 4683−4691

$$\frac{v_s}{v_0} = \frac{1}{1 + \frac{[I]}{K_i^{*app}}} \quad (4)$$

Finally, k_5 was calculated using eq 5:

$$k_{obs} = k_6 + \frac{k_5}{1 + K_i^{app}/[I]} \quad (5)$$

The dissociation rate constant of the inhibitor from EI* ($k_{off} = k_6$) was also determined by directly monitoring the release of the inhibitor from the complex using a recently described method that utilizes [^{32}P]NAD$^+$.[25] In general, 500 μL of reaction mixture containing 15 μM InhA, 20 μM NAD$^+$, [^{32}P]NAD$^+$, and 200 μM inhibitor in the reaction buffer mentioned above was loaded onto a spin column followed by a 2 min centrifugation at 2500 rpm. The purified ternary complex solution was rapidly diluted into 60 mL of the same reaction buffer at different temperatures to initiate ligand dissociation. Subsequently, 600 μL aliquots from the diluted mixture were collected as a function of time and immediately loaded onto an ultrafiltration concentrator (Satorious, 10 kDa) that was centrifuged at 13400 rpm for 90 s. The amount of [^{32}P]NAD$^+$ in the flow-through was then quantified using a scintillation counter (LS5801). The inhibitor dissociation rate constant k_{off} was obtained by fitting the data to eq 6

$$C(t) = C(0) + C_{max}(1 - e^{k_{off}t}) \quad (6)$$

where $C(t)$ and $C(0)$ are the radioactive counts at time t and time zero, respectively, C_{max} is the maximal number of radioactive counts, and k_{off} is the inhibitor dissociation rate constant.

RESULTS

Transition State to Isomerization of the Substrate Binding Loop. To design inhibitors with altered residence times on the enzyme, it is important to understand the protein−protein and protein−inhibitor interactions that change as the open and closed states interconvert. We previously calculated pathways and corresponding free energy landscapes [potentials of mean force (PMFs)] for InhA loop isomerization.[18] Here, free energies are again calculated as a function of these two global measures of SBL geometry, step and shear torsions (Figure S1 of the Supporting Information). Rapid-reversible complexes of InhA exhibit two types of free energy landscape, either preferring the open state or having little preference and a relatively flat landscape. In contrast, slow-onset inhibition complexes have a more stable closed state with a significantly higher energy barrier between the open and closed states. For example, the free energy for loop isomerization in the slow-onset InhA^{WT}−NAD$^+$−PT70 ternary complex shows a barrier of ∼6 kcal/mol at the saddle point (hereafter simply termed the transition state), compared to nearly no barrier when PT70 is replaced with the rapid-reversible inhibitor triclosan (Figure 1). In addition to this consistency with kinetic data, these computed energy landscapes are also supported by crystallographic data; the global minimum on the PT70 landscape is the closed form that is seen in crystal structures of this complex,[14] while the flat triclosan-bound landscape is consistent with the lack of electron density seen for the triclosan-bound SBL loop[12] (Figure 1).

Although the energy values on the landscapes are likely to be only qualitative,[18] an important characteristic of the simulation data is that structures near the PMF transition state can be

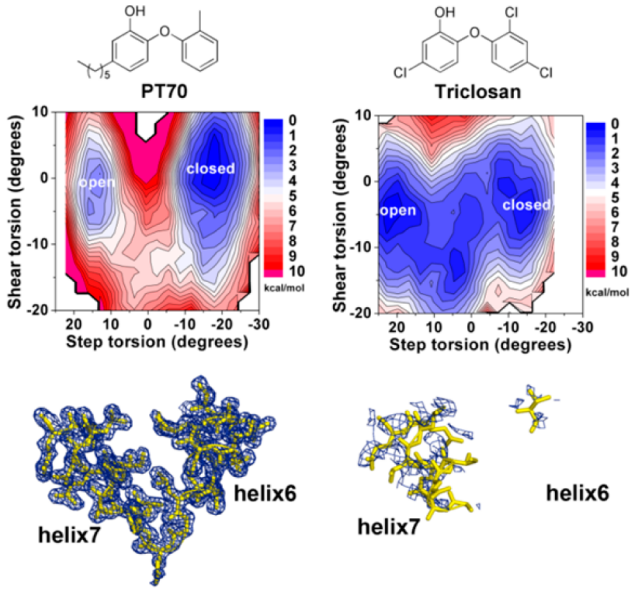

Figure 1. Inhibitors, free energy landscapes for SBL isomerization, and SBL crystallographic electron densities ($2F_o - F_c$, 1σ contour). Left: PT70, with the global free energy minimum in the closed basin, and ordered, closed SBL in the crystal.[14] Right: triclosan, with a relatively flat landscape and weak density for the SBL.[12]

extracted from the simulations and analyzed to gain insight into the atomic-level interactions that give rise to the slow-onset behavior. Analysis of transition state structures from the InhA^{WT}−NAD$^+$−PT70 landscape in Figure 1 revealed that hydrophobic side chains on SBL helices 6 and 7 (specifically Met199, Val203, Ala211, and Ile215) slide past each other near the midpoint of isomerization (Figure 2). The distance between backbone atoms of Val203 on helix 6 and Ile215 on helix 7 follows a nonlinear path during SBL opening, initially approaching but then temporarily moving apart near the transition state before resuming their approach as the loop continues to open (Figure 2). This suggests that the side chains on each helix approach to form a van der Waals contact, but the direct path to SBL isomerization has a steric clash. This behavior as Ile215 passes Val203 is similar to a coin purse ball clasp that also employs a steric clash to stay closed (Figure S2 of the Supporting Information). We speculate that these steric clashes, amplified by crowding from the nearby inhibitor, impede the conformational changes between open and closed states for the InhA^{WT}−NAD$^+$−PT70 slow-onset inhibition complex.

Connecting the Steric Clash to the Isomerization Energy Barrier. If the steric clash between the SBL helices is responsible for the energy barrier to isomerization, replacing residues Val203 or Ile215 with a smaller side chain (Ala) should decrease the energy barrier at the transition state. We mapped the pathways and free energy landscapes of the ternary complex for both mutants (InhA^{V203A}−NAD$^+$−PT70 and InhA^{I215A}−NAD$^+$−PT70). As predicted, replacement of either side chain with alanine now permits the close approach of helices 6 and 7 during isomerization (Figure S3 of the Supporting Information), suggesting that the clash was eliminated. Importantly, the free energy landscapes also change in the manner predicted by our model. As shown in panels A and C of Figure 3, the energy landscapes for both mutants are qualitatively flatter than that of the InhA^{WT}−NAD$^+$−PT70 complex in Figure 1. Subtracting

DOI: 10.1021/acs.biochem.5b00284
Biochemistry 2015, 54, 4683−4691

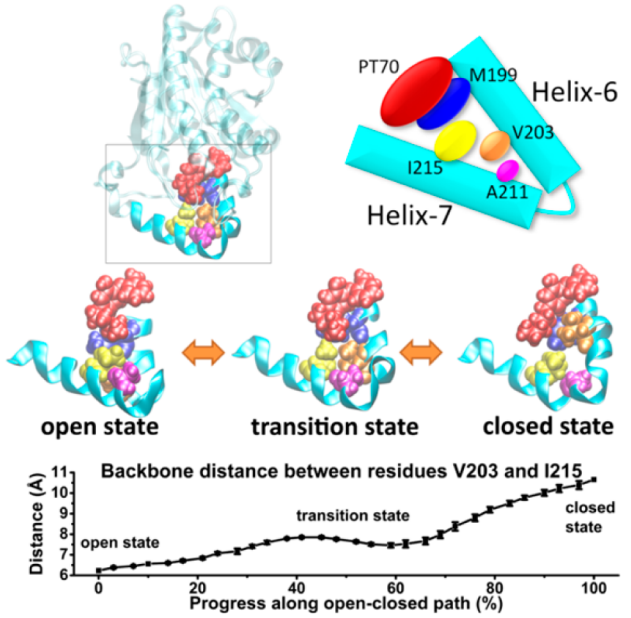

Figure 2. Isomerization of the SBL in InhA^{WT}–NAD$^+$–PT70 simulations. (Top) Schematic of key residues on SBL helices 6 and 7 (region outlined in the box). The color scheme matches that used in the structure images. (Middle) Side chains of M199, V203, and I215 are crowded by PT70 and encounter a steric clash during SBL isomerization. (Bottom) Distance between V203 and I215 backbone atoms during isomerization. The helices approach during SBL opening and then move apart to resolve the clash prior to further opening.

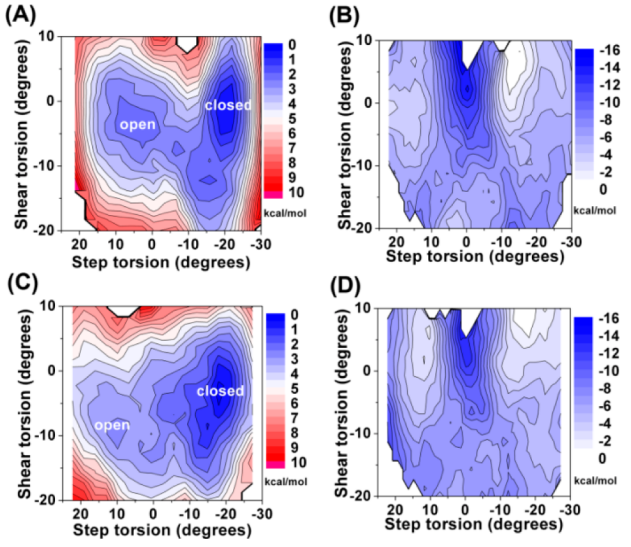

Figure 3. Free energy landscapes for SBL loop isomerization for the InhA–NAD$^+$–PT70 complex with (A) V203A and (C) I215A mutations. The landscapes to the right (B and D) show the difference between the plot on the left and that from WT InhA with PT70 (Figure 1). The change is predominantly in the transition state region near the 0° step torsion.

the mutant landscape from that of the wild type (Figure 3B,D) indicates that the influence of the mutation in both cases is dominant near the transition state, while the relative stabilities of the open and closed minima are largely unchanged. When either one of the clash partners is reduced in size, the energy landscape for mutant InhA with PT70 (Figure 3) is comparable to that seen for the wild-type enzyme with triclosan, a rapid-reversible complex (Figure 1).

The PMFs provide the relative free energy during loop isomerization, but the zero of free energy on each PMF is arbitrary. This complicates quantitative comparison of different surfaces. Changes to the apparent energy barrier could arise from the changes at either the transition states or the ground states. Additional calculations are required to confirm that the flatter landscapes were obtained for the reasons that the model predicted. We therefore performed thermodynamic integration (TI) to calculate the relative binding free energy of PT70 between wild-type and mutant InhA ($\Delta\Delta G$WT → mutant), both in the closed state (Table S3 and Figure S4 of the Supporting Information). This allows calibration of different isomerization PMFs to the same energy scale, allowing us to use an absolute scale for the calculated impact of the mutations on specific regions of the energy landscape. For Ile215, a small ground state effect is expected, because the Ile215 side chain has only weak interactions with the end of the PT70 alkyl tail. A value of 0.3 ± 0.1 kcal/mol was obtained for the I215A mutation, confirming that the mutation modestly destabilizes inhibitor binding. Val203 interacts with the diphenyl ether moiety of the inhibitor, and as expected, the V203A mutation has a somewhat larger ground state effect, weakening binding of PT70 by 0.5 ± 0.1 kcal/mol. To more easily visualize the differences between multiple systems, we converted the 2D PMFs (that use structural measures for reaction coordinates) to 1D free energy as a function of isomerization progress (Figure S5 of the Supporting Information). The calibrated 1D PMFs demonstrate that the I215A and V203A mutations have a minor influence on the minima but reduce the energy barrier for SBL opening from 6.1 to ∼2.4 kcal/mol (Figure S6 of the Supporting Information).

When combined, these calculations of free energy differences for loop isomerization and side chain mutation confirm that the V203A and I215A mutants change the SBL isomerization free energy profile mainly by decreasing the energy of the transition state. This supports our hypothesis that the steric clashes between residues Val203 and Ile215 control the rate of SBL isomerization. The observation that PT70 is able to increase the energy barrier in wild-type InhA (Figure 1, PT70 vs triclosan) but that PT70 does so less effectively when the side chains for the clash barrier are reduced in size (Figure 1 vs Figure 3A,C) suggests that the role of the inhibitor in slow-onset kinetics is indirect; the characteristic of inhibitors that confers slow-onset kinetics appears to be the ability to crowd the SBL and magnify the steric clash between helices 6 and 7 during SBL isomerization. Slow inhibitor dissociation is thus a result of the combination of a bulky side chain on each helix, along with steric crowding by the nearby inhibitor. Importantly, changing any of these three components results in significant modulation of the energy barrier to SBL isomerization.

Validating the Energy Landscapes: Crystal Structures and Kinetic Experiments for InhA V203A and I215A with PT70. As shown in Figure 3, the free energy profiles for the V203A and I215A ternary complexes are both significantly flatter than for wild-type InhA (Figure 1). Although PT70 is a slow-onset inhibitor of wild-type InhA, both mutations result in energy landscapes for PT70 that appear to be qualitatively similar to the landscapes seen for rapid-reversible inhibitors such as triclosan (Figure 1). Our data therefore suggest that reducing the size of the steric clash pair would have a similar effect on SBL flexibility as seen in rapid-reversible inhibitors. As

DOI: 10.1021/acs.biochem.5b00284
Biochemistry 2015, 54, 4683–4691

stated above, whereas in the presence of a large energy barrier the SBL adopts a defined conformation, flat energy landscapes correlate with weak or absent electron density corresponding to the SBL, indicative of conformational disorder. We determined crystal structures for the InhA^{V203A}–NAD$^+$–PT70 and InhA^{I215A}–NAD$^+$–PT70 ternary complexes. Although binding of PT70 induces loop closing for WT InhA,[14,18] the loop remains dynamic when either residue involved in the steric clash is reduced in size, and only weak electron density is observed for helices 6 and 7 (Figure 4 and Table S4 of the Supporting Information, with additional analysis of SBL variation among different monomers in the unit cell shown in Figure S7 of the Supporting Information), similar to that seen in the wild-type ternary complex with the rapid-reversible inhibitor triclosan (Figure 1).

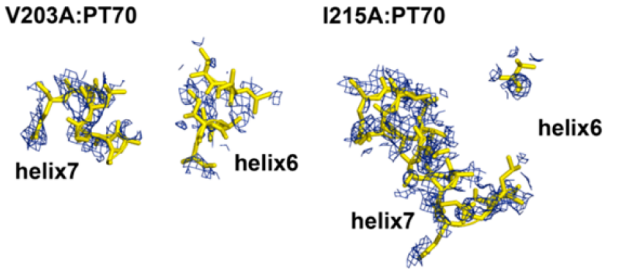

Figure 4. Crystallographic SBL electron density ($2F_o - F_c$, 1σ contour) for (left) the InhA^{V203A}–NAD$^+$–PT70 complex and (right) the InhA^{I215A}–NAD$^+$–PT70 complex, shown in the same view as in Figure 1. As predicted by the free energy landscapes, PT70 binding does not induce loop ordering in either mutant.

Thermodynamic and kinetic characteristics of inhibitor binding were measured for the V203A and I215A variants with PT70 (Table 1). The I215A and V203A mutations resulted in a <2-fold reduction in k_{cat}/K_m for the uninhibited enzyme, suggesting a minimal role in substrate binding and release. We compared the predicted and measured impact of the mutations on inhibitor affinity and on the relative free energy of open and closed forms, along with the relative affinities of PT70 and PT163. The TI binding affinity calculations suggested that the mutations modestly weaken PT70 binding by 0.3 and 0.5 kcal/mol for I215A and V203A, respectively (Table S3 of the Supporting Information). These are in reasonable agreement with experimental ground state binding free energy reductions (from K_i^{*app}) of 0.9 and 0.8 kcal/mol for the same mutations (Table 1). Moreover, both K_i and K_i^* increase with these mutations, such that K_i/K_i^* values are similar for all three systems, with corresponding $\Delta\Delta G$ values of 1.41, 1.55, and 0.92 for WT, I215A, and V203A, respectively (Table 1). This suggests that the relative stabilities of EI and EI* are not significantly affected by these mutations. The trends are comparable to the predicted relative stabilities of EI and EI* [$\Delta\Delta G$ values of 3.4, 2.4, and 1.0 for WT, I215A, and V203A, respectively (Figure S6 of the Supporting Information), though the computational values are more qualitative because they are obtained from the differences between the end points of loop isomerization free energy profiles (Figure S6 of the Supporting Information). In terms of kinetics, a 3–4-fold decrease in the residence time of PT70 was observed for these variants compared to that of wild-type InhA (Table 1). These experimental kinetic and crystallographic observations support the computational prediction that the

Table 1. Experimental Kinetic and Thermodynamic Parameters for Binding of PT70 and PT163 to WT and Mutant InhA

	k_{cat} (min^{-1})	K_m (μM)	k_{cat}/K_m (μM^{-1} min^{-1})	k_5 (min^{-1})	k_6 (min^{-1})	t_R ($1/k_6$) (min)	t_R ([^{32}P]NAD) (min)	K_i^{app} (nM)	K_i^{*app} (nM)	K_i^{app}/K_i^{*app}	$\Delta\Delta G$ (kcal mol^{-1})
InhA^{WT}	278 ± 26	27 ± 7	10 ± 3								
PT70				0.40 ± 0.01	0.025 ± 0.002	40 ± 2	37 ± 2	256.2 ± 38.0	23.7 ± 3.6	10.8	1.41
PT163				0.44 ± 0.06	0.011 ± 0.001	94 ± 3	114 ± 18	8382.9 ± 365.2	185.2 ± 8.6	45.3	2.26
InhA^{I215A}	109 ± 5	13 ± 2	8.4 ± 1								
PT70				0.4	0.071[a]	14	14 ± 1	1570.6[b]	114.3 ± 7.5	13.7	1.55
PT163				0.78 ± 0.14	0.009 ± 0.001	109 ± 2	111 ± 10	20640 ± 1865	229.2 ± 9.4	90.1	2.67
InhA^{V203A}	78 ± 7	13 ± 3	6 ± 1								
PT70				0.7	0.1[a]	10	11 ± 1	427.5[b]	91.3 ± 3.7	4.7	0.92

[a]Value determined from a single progress curve. [b]K_i^{app} calculated at a fixed inhibitor concentration using eq 3.

DOI: 10.1021/acs.biochem.5b00284
Biochemistry 2015, 54, 4683–4691

steric clash between helices 6 and 7 is a controlling factor in the SBL isomerization and ligand residence time.

Reintroducing Steric Clashes To Restore the Energy Barrier. If our model is correct, the reduced residence time observed with the V203A and I215A mutants may be recoverable if steric clashes at the transition state are restored. We focused on the alkyl tail of PT70, where we speculated that an appropriately bulky group could intensify crowding of the binding loop during isomerization and compensate for the smaller side chain in the I215A mutant InhA. We designed the inhibitor 5-[(4-phenyl-1*H*-1,2,3-triazol-1-yl)methyl]-2-(*o*-tolyloxy)phenol [PT163 (Figure 5A)] with the goal being

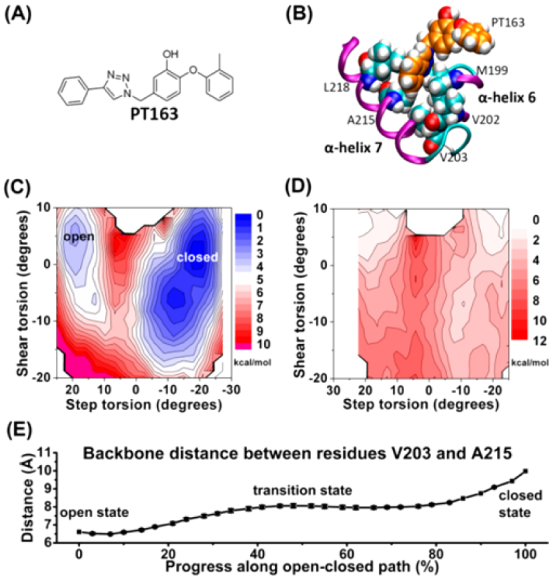

Figure 5. Data from InhA^{I215A}–NAD$^+$–PT163 simulations. (A) PT163 structure. (B) Docked complex, with PT163 carbon atoms colored orange. (C) PMF for SBL isomerization. (D) Difference between this profile with PT163 and that with PT70 (Figure 4). (E) Backbone distance between residues Val203 and Ala215.

that the phenyl moiety would play a role in producing a steric clash with Val203 in the I215A mutant, analogous to that of the Ile215 side chain in the wild type. Docking calculations suggested that the phenyl group on the PT163 tail could fit into the cavity near V202, A215, and L218 (Figure 5B); thus, we proceeded with mapping the SBL isomerization pathway and free energy landscape for the InhA^{I215A}–NAD$^+$–PT163 complex (Figure 5C).

Consistent with the design goal, the barrier between closed and open forms of the I215A mutant is significantly higher with PT163 than with PT70 (Figure 5D). Evidence that the increased energy barrier arises from the designed crowding of the SBL is shown in Figure 5E, where we show that the distance between helices 6 and 7 regains the bulge that was seen with PT70 in the wild type (Figure 2) but was lost for PT70 and this mutant (Figure S3 of the Supporting Information). The results demonstrate that it is possible to rationally modify an inhibitor to magnify a steric clash in the enzyme during the isomerization that accompanies inhibition.

Because the additional bulk of PT163 makes more extensive contact with surrounding residues, we again investigated whether the affinity for the closed form was impacted by the change. We calculated the relative binding free energy between PT163 and PT70 in the I215A mutant, finding that the overall binding free energy of PT163 is weakened by 5.6 ± 0.8 kcal mol^{-1} compared to that of PT70 (Table 1). Using the TI data to calibrate the PMF curves suggests that PT163 indeed achieves the goal of destabilizing the transition state to SBL isomerization, although overall binding is also weakened (Figure S8 of the Supporting Information). Weaker overall binding is not surprising, because the selection of the ligand was based on the ability to crowd the SBL during isomerization, and binding affinity was not explicitly considered.

Experimental Measurement of Binding Parameters for PT163. To experimentally validate the impact of the design on ligand binding kinetics, characteristics of binding of PT163 and PT70 to I215A mutant InhA were measured (Table 1). Comparing K_i^{*app} values confirms the computational prediction of reduced overall affinity for EI* with PT163; K_i^{*app} increased from 114 nM for I215A/PT70 to 229 nM for I215A/PT163. A larger impact is seen in the experimental measurement for binding to WT InhA, where K_i^{*app} has increased from 24 nM (PT70) to 185 nM (PT163) for WT, i.e., a change of 8-fold compared to 2-fold for PT70-PT163 with I215A. The weaker binding of PT163 versus that of PT70 is more pronounced in the calculations, probably because of the use of a docked model for calculation of PT163 affinity while a crystal structure was used for PT70.

We also compared the relative stability of EI and EI* for PT163/I215A. Although the simulations predict somewhat larger relative stabilities for the closed loop with both inhibitors, both MD and experiment are in agreement that PT163 has ∼1 kcal greater relative affinity for the closed form (EI*) than does PT70. The MD calculations predicted a $\Delta\Delta G$ of 4.0 kcal/mol for PT163 (Figure S8 of the Supporting Information), 1.6 kcal/mol larger than the PT70 value presented above. Experimentally, the $\Delta\Delta G$ value for PT163 is 2.7 kcal/mol, which is 1.1 kcal/mol larger than that of PT70.

To test the computational prediction of an increased residence time for PT163, k_{off} values for PT70 and PT163 with InhA^{I215A} were measured. Remarkably, an 8-fold increase in residence time was observed for PT163 (111 min) versus PT70 with InhA^{I215A} (14 min) (Table S6 of the Supporting Information)].

We next determined the crystal structure for the InhA^{I215A}–NAD$^+$–PT163 ternary complex (Table S5 of the Supporting Information) and confirmed that PT163 binding is able to induce ordering of the SBL with this mutant (Figure 6A), which did not occur with PT70 (Figure 4). Moreover, the structure confirmed that PT163 indeed binds as predicted in

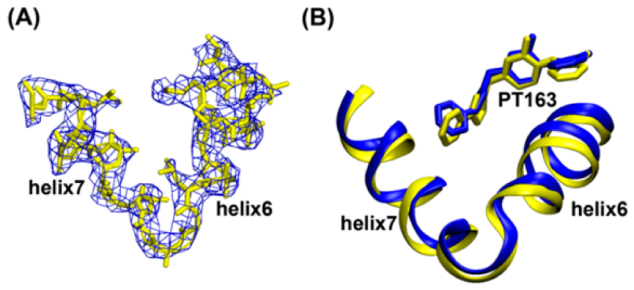

Figure 6. (A) Crystallographic SBL electron density ($2F_o - F_c$, 1σ contour) for the InhA^{I215A}–NAD$^+$–PT163 complex. Unlike PT70 binding (Figure 4), PT163 binding results in an ordered SBL for this mutant. (B) Comparison of predicted (yellow) and crystallographic (blue) PT163 binding poses.

DOI: 10.1021/acs.biochem.5b00284
Biochemistry 2015, 54, 4683–4691

the region near Val203 (Figure 6B). This position also serves to intensify the steric clash even for wild-type InhA, though the effect is smaller than for the mutant (37 and 114 min for PT70 and PT163, respectively).

Taken together, the computational and experimental results confirm the design goal; the bulky group that was added to the ligand counteracts the effect of the alanine mutation and results in an ordered, closed SBL and increases the energy barrier to ligand dissociation, and longer residence time. The results reinforce our confidence that a steric clash between the two helices of the active site loop is the source of the barrier controlling conformational changes between open and closed states, and that future rational design efforts could include optimization of the effect of the inhibitor on binding site isomerization in addition to thermodynamic binding affinity.

Transferability of the Model to Other Pathogens. We predict a similar potential for steric hindrance, and thus an opportunity for time-dependent inhibition, in other FabI enzymes. We superimposed structures of InhA and other FabIs (*Escherichia coli*,[15] *F. tularensis*,[26] *Staphylococcus aureus*,[27] *Bacillus subtilis*,[28] *Helicobacter pylori*,[29] and *Bacillus anthracis*[30]) and found conserved residues Ala and Phe corresponding to residues Val203 and Ile215 of InhA, respectively (Figure 7). In

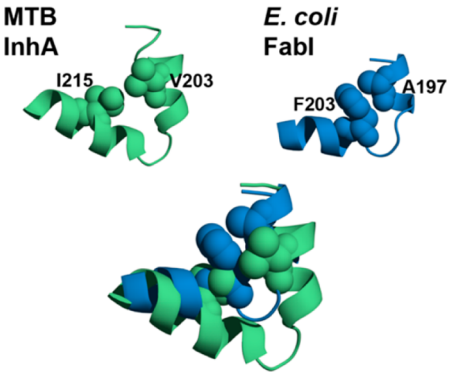

Figure 7. Comparison of structures of the substrate binding loops from *M. tuberculosis* InhA and *E. coli* FabI (Protein Data Bank entry 1QSG). I215 and V203 in InhA may have comparable residues in other FabI enzymes, with the potential for steric clash modulated by rationally designed inhibitors.

cases in which slow-onset inhibitors are known, structures of the complexes have a closed, ordered helix 6, while helix 6 appears to be disordered with rapid-reversible inhibitors. Because the Ala and Phe are conserved among all of these FabI sequences, we speculate that optimizing inhibitors to constrain Phe203 and Ala197 (*E. coli* numbering) and produce additional steric clash might help control time-dependent inhibition in these FabIs. Future simulation, crystallographic, and kinetics studies will explore this hypothesis.

Perspective and Limitations for Designing New Inhibitors. During lead optimization, especially for tight binding inhibitors, it can be challenging to increase the residence time by solely considering improving the binding affinity. Increasing the free energy barrier by introducing unfavorable interactions during the active site loop isomerization may be a more feasible approach. Although one can apply the protocol we present here to screen candidate inhibitors for significant energy barriers prior to *in vitro* and *in vivo* experiments, one should also consider potential limitations.

First, it is always challenging to describe complex dynamics using a small number of descriptors, because molecular motion can be inherently highly dimensional. Here, structural analysis of the isomerization pathway was used to select progress variables (reaction coordinates). If these variables do not accurately track the motion that corresponds to the slowest event, free energy mapping as performed here may not deliver an accurate energy barrier or transition state structural model.[31] Another limitation related to the high dimensionality of the dynamics is that there is likely an ensemble of paths for active site loop isomerization, contributing varying amounts to the apparent rate. Increasing the barrier along one low-energy pathway may lead to increased flux along a different path, involving interactions other than those identified from the original path. Furthermore, the energy barriers obtained from the PMF do not directly correspond to rate constants, and more complex approaches would be needed to accurately predict kinetics.[32,33] Thus, the PMF trends are most useful as a qualitative predictor of the effect of changes to the system, and as a method for obtaining an atomistic model for the transition state to isomerization. Finally, as seen in the proof of concept work presented here, it can be challenging to modulate the interactions at the transition state without impacting overall binding affinity. Careful structural visualization may provide guidance, and as described above, binding affinity calculations can be used to help separate the effects.

CONCLUSION

In summary, we showed that computationally mapping the pathway of the loop isomerization allowed us to obtain models of structures near the transition state for the conformational change. Structural analysis then provided insight into the specific interactions that modulate the energy barrier. We hypothesize that a steric clash between side chains on two helices that pass closely during loop isomerization is responsible for the binding kinetics. The proximity of this hydrophobic cluster to the ligand binding pocket and the resulting potential for the ligand to crowd the loop and amplify the clash result in the experimentally observed sensitivity of residence time to inhibitor structure. Our model is strongly supported by our ability to rationally remove the energy barrier through directed protein mutations and then recover it with a rationally redesigned ligand. Crystallographic studies also confirmed our prediction that mutating the steric clash residues strongly impacts SBL flexibility. This insight into how a ligand can modulate protein steric clashes dominating the kinetics of induced fit should be valuable for future efforts at further optimizing inhibitor residence times for InhA or work to improve ligand ADME properties while retaining long residence times. Examination of homologous FabI sequences in other pathogens reveals similar interactions between the corresponding loops, suggesting that this may be a general approach to developing slow-onset inhibitors of this critical pathway.

ASSOCIATED CONTENT

Supporting Information

Detailed methods, crystallographic refinement statistics, energy function parameters for inhibitors, thermodynamic integration results, experimental kinetics data, definition of reaction coordinates, additional simulation analysis data for mutants, analysis of reaction coordinate values obtained from crystal structures, and 1D PMFs. The Supporting Information is

DOI: 10.1021/acs.biochem.5b00284
Biochemistry 2015, 54, 4683−4691

available free of charge on the ACS Publications website at DOI: 10.1021/acs.biochem.5b00284.

AUTHOR INFORMATION

Corresponding Authors

*E-mail: peter.tonge@stonybrook.edu.

*E-mail: carlos.simmerling@stonybrook.edu.

Funding

This work was supported by Grant GM102864 from the National Institutes of Health to P.J.T. and support from Henry and Marsha Laufer to C.S. X-ray data were measured at the National Synchrotron Light Source, financial support for which comes principally from the U.S. Department of Energy and from National Center for Research Resources Grant P41RR012408. This research was also supported in part by the National Science Foundation (NSF) through TeraGrid resources provided by NICS via Grants TG-CHE100107 and TG-MCA02N028 to C.S. and an NSF Petascale Computational Resource (PRAC) Award (OCI-1036208).

Notes

The authors declare no competing financial interest.

DEDICATION

This article is dedicated to Professor Iwao Ojima on the occasion of his 70th birthday.

ABBREVIATIONS

INH, isoniazid; SBL, substrate binding loop; NEB, nudged elastic band; PMF, potential of mean force; TI, thermodynamic integration; WT, wild type.

REFERENCES

(1) Vilums, M., Zweemer, A. J. M., Yu, Z., de Vries, H., Hillger, J. M., Wapenaar, H., Bollen, I. A. E., Barmare, F., Gross, R., Clemens, J., Krenitsky, P., Brussee, J., Stamos, D., Saunders, J., Heitman, L. H., and Ijzerman, A. P. (2013) Structure−Kinetic Relationships—An Overlooked Parameter in Hit-to-Lead Optimization: A Case of Cyclopentylamines as Chemokine Receptor 2 Antagonists. *J. Med. Chem. 56*, 7706−7714.

(2) Schneider, E. V., Böttcher, J., Huber, R., Maskos, K., and Neumann, L. (2013) Structure−kinetic relationship study of CDK8/CycC specific compounds. *Proc. Natl. Acad. Sci. U. S. A. 110*, 8081−8086.

(3) Shapiro, A. B., Gao, N., Hajec, L., and McKinney, D. C. (2012) Time-dependent, reversible, oxaborole inhibition of Escherichia coli leucyl-tRNA synthetase measured with a continuous fluorescence assay. *Anal. Biochem. 431*, 48−53.

(4) Frantom, P. A., Coward, J. K., and Blanchard, J. S. (2010) UDP-(5F)-GlcNAc Acts as a Slow-Binding Inhibitor of MshA, a Retaining Glycosyltransferase. *J. Am. Chem. Soc. 132*, 6626−6627.

(5) Swinney, D. (2008) Applications of Binding Kinetics to Drug Discovery. *Pharm. Med. 22*, 23−34.

(6) Copeland, R. A., Pompliano, D. L., and Meek, T. D. (2006) Drug-target residence time and its implications for lead optimization. *Nat. Rev. Drug Discovery 5*, 730−739.

(7) Tummino, P. J., and Copeland, R. A. (2008) Residence time of receptor-ligand complexes and its effect on biological function. *Biochemistry 47*, 5481−5492.

(8) Lu, H., England, K., am Ende, C., Truglio, J. J., Luckner, S., Reddy, B. G., Marlenee, N. L., Knudson, S. E., Knudson, D. L., Bowen, R. A., Kisker, C., Slayden, R. A., and Tonge, P. J. (2009) Slow-onset inhibition of the FabI enoyl reductase from *Francisella tularensis*: residence time and in vivo activity. *ACS Chem. Biol. 4*, 221−231.

(9) Lu, H., and Tonge, P. J. (2010) Drug-target residence time: critical information for lead optimization. *Curr. Opin. Chem. Biol. 14*, 467−474.

(10) Otwinowski, Z., and Minor, W. (1997) Processing of X-ray diffraction data collected in oscillation mode. In *Methods in Enzymology* (Carter, C. W., Jr., Ed.) pp 307−326, Academic Press, San Diego.

(11) Rawat, R., Whitty, A., and Tonge, P. J. (2003) The isoniazid-NAD adduct is a slow, tight-binding inhibitor of InhA, the Mycobacterium tuberculosis enoyl reductase: Adduct affinity and drug resistance. *Proc. Natl. Acad. Sci. U. S. A. 100*, 13881−13886.

(12) Sullivan, T. J., Truglio, J. J., Boyne, M. E., Novichenok, P., Zhang, X., Stratton, C. F., Li, H. J., Kaur, T., Amin, A., Johnson, F., Slayden, R. A., Kisker, C., and Tonge, P. J. (2006) High affinity InhA inhibitors with activity against drug-resistant strains of Mycobacterium tuberculosis. *ACS Chem. Biol. 1*, 43−53.

(13) Pan, P., and Tonge, P. J. (2012) Targeting InhA, the FASII Enoyl-ACP Reductase: SAR Studies on Novel Inhibitor Scaffolds. *Current Topics in Medicinal Chemistry*, Vol. *12*, pp 672−693, Wiley, New York.

(14) Luckner, S. R., Liu, N., am Ende, C. W., Tonge, P. J., and Kisker, C. (2010) A slow, tight binding inhibitor of InhA, the enoyl-acyl carrier protein reductase from Mycobacterium tuberculosis. *J. Biol. Chem. 285*, 14330−14337.

(15) Stewart, M. J., Parikh, S., Xiao, G., Tonge, P. J., and Kisker, C. (1999) Structural basis and mechanism of enoyl reductase inhibition by triclosan. *J. Mol. Biol. 290*, 859−865.

(16) Mathews, D. H., and Case, D. A. (2006) Nudged Elastic Band Calculation of Minimal Energy Paths for the Conformational Change of a GG Non-canonical Pair. *J. Mol. Biol. 357*, 1683−1693.

(17) Bergonzo, C., Campbell, A. J., Walker, R. C., and Simmerling, C. (2009) A Partial Nudged Elastic Band Implementation for Use with Large or Explicitly Solvated Systems. *Int. J. Quantum Chem. 109*, 3781.

(18) Li, H. J., Lai, C. T., Pan, P., Yu, W., Liu, N., Bommineni, G. R., Garcia-Diaz, M., Simmerling, C., and Tonge, P. J. (2014) A structural and energetic model for the slow-onset inhibition of the Mycobacterium tuberculosis enoyl-ACP reductase InhA. *ACS Chem. Biol. 9*, 986−993.

(19) Case, D. A., Cheatham, T. E., Darden, T., Gohlke, H., Luo, R., Merz, K. M., Onufriev, A., Simmerling, C., Wang, B., and Woods, R. J. (2005) The Amber biomolecular simulation programs. *J. Comput. Chem. 26*, 1668−1688.

(20) Hornak, V., Abel, R., Okur, A., Strockbine, B., Roitberg, A., and Simmerling, C. (2006) Comparison of multiple Amber force fields and development of improved protein backbone parameters. *Proteins: Struct., Funct., Genet. 65*, 712−725.

(21) Wang, J., Wolf, R. M., Caldwell, J. W., Kollman, P. A., and Case, D. A. (2004) Development and testing of a general amber force field. *J. Comput. Chem. 25*, 1157−1174.

(22) Lang, P. T., Brozell, S. R., Mukherjee, S., Pettersen, E. F., Meng, E. C., Thomas, V., Rizzo, R. C., Case, D. A., James, T. L., and Kuntz, I. D. (2009) DOCK 6: combining techniques to model RNA-small molecule complexes. *RNA 15*, 1219−1230.

(23) Morrison, J. F., and Walsh, C. T. (1988) The behavior and significance of slow-binding enzyme inhibitors. *Adv. Enzymol. Relat. Areas Mol. Biol. 61*, 201−301.

(24) Copeland, R. A. (2005) *Evaluation of enzyme inhibitors in drug discovery: a guide for medicinal chemists and pharmacologists*, p 538, Wiley & Sons, Inc., New York.

(25) Yu, W., Neckles, C., Chang, A., Bommineni, G. R., Spagnuolo, L., Zhang, Z., Liu, N., Lai, C., Truglio, J., and Tonge, P. J. (2015) A [P]NAD-based method to identify and quantitate long residence time enoyl-acyl carrier protein reductase inhibitors. *Anal. Biochem. 474C*, 40−49.

(26) Mehboob, S., Truong, K., Santarsiero, B. D., and Johnson, M. E. (2010) Structure of the Francisella tularensis enoyl-acyl carrier protein reductase (FabI) in complex with NAD+ and triclosan. *Acta Crystallogr., Sect. F: Struct. Biol. Cryst. Commun. 66*, 1436−1440.

(27) Priyadarshi, A., Kim, E. E., and Hwang, K. Y. (2010) Structural insights into Staphylococcus aureus enoyl-ACP reductase (FabI), in

DOI: 10.1021/acs.biochem.5b00284
Biochemistry 2015, 54, 4683−4691

complex with NADP and triclosan. *Proteins: Struct., Funct., Genet. 78*, 480−486.
(28) Kim, K.-H., Ha, B. H., Kim, S. J., Hong, S. K., Hwang, K. Y., and Kim, E. E. (2011) Crystal Structures of Enoyl-ACP Reductases I (FabI) and III (FabL) from B. subtilis. *J. Mol. Biol. 406*, 403−415.
(29) Lee, H. H., Moon, J., and Suh, S. W. (2007) Crystal structure of the Helicobacter pylori enoyl-acyl carrier protein reductase in complex with hydroxydiphenyl ether compounds, triclosan and diclosan. *Proteins: Struct., Funct., Genet. 69*, 691−694.
(30) Tipparaju, S. K., Mulhearn, D. C., Klein, G. M., Chen, Y., Tapadar, S., Bishop, M. H., Yang, S., Chen, J., Ghassemi, M., Santarsiero, B. D., Cook, J. L., Johlfs, M., Mesecar, A. D., Johnson, M. E., and Kozikowski, A. P. (2008) Design and Synthesis of Aryl Ether Inhibitors of the Bacillus Anthracis Enoyl-ACP Reductase. *ChemMedChem 3*, 1250−1268.
(31) Zheng, L., Chen, M., and Yang, W. (2009) Simultaneous escaping of explicit and hidden free energy barriers: application of the orthogonal space random walk strategy in generalized ensemble based conformational sampling. *J. Chem. Phys. 130*, 234105.
(32) Faradjian, A. K., and Elber, R. (2004) Computing time scales from reaction coordinates by milestoning. *J. Chem. Phys. 120*, 10880−10889.
(33) Elber, R. (2007) A Milestoning Study of the Kinetics of an Allosteric Transition: Atomically Detailed Simulations of Deoxy Scapharca Hemoglobin. *Biophys. J. 92*, L85−L87.

DOI: 10.1021/acs.biochem.5b00284
Biochemistry 2015, 54, 4683−4691